Protection of cultural heritage from earthquakes: The NIKER project and the related research at UMinho

Daniel V. Oliveira[1], Paulo B. Lourenço[2]
[1] *ISISE, University of Minho, Department of Civil Engineering, Guimarães, Portugal; danvco@civil.uminho.pt*
[2] *ISISE, University of Minho, Department of Civil Engineering, Guimarães, Portugal; pbl@civil.uminho.pt*

ABSTRACT: The European Commission has recently funded a major research project (NIKER) which aimed at developing an integrated methodology for the systemic improvement of the seismic behaviour of cultural heritage assets. This paper provides an overview of the project and presents the most relevant contributions from University of Minho as partner of the project.

KEYWORDS: Cultural heritage; earthquakes; masonry; experiments; numerical modelling

1 INTRODUCTION

Potential damages to cultural heritage assets due to earthquakes are currently too high, commonly due to their intrinsic vulnerability and to the fact that most of the technologies currently applied are excessively intrusive, cost-inefficient and often unsuccessful. Given this, the need to develop proper strategies to mitigate the seismic risk is a key issue in research.

The NIKER project, coordinated by University of Padova, Italy, is a European project aiming at the protection of Cultural Heritage from earthquake-induced risk, by developing and validating innovative materials and technologies for systemic improvement of seismic behaviour of cultural heritage assets. The NIKER consortium was composed by 18 partners with different expertizes from 12 countries of the Mediterranean basin, which run from 2010 to 2012 [1]. The project tackled the problem of earthquake-impact on cultural heritage assets starting from consideration that efficient protection can only be achieved on the basis of the "minimum intervention" approach. To achieve this purpose, the project research was organized into 10 work-packages and the following main steps were then established, see also Figure 1:

- creation of a database of earthquake-induced failure mechanisms, construction types and materials, intervention and assessment techniques;
- extensive experimental testing, numerical simulations and derivation of design methods for vertical and horizontal structural elements, for connections, and for the overall seismic behaviour of buildings;
- development of knowledge-based assessment procedures, also through real case-study application of investigation and monitoring techniques.

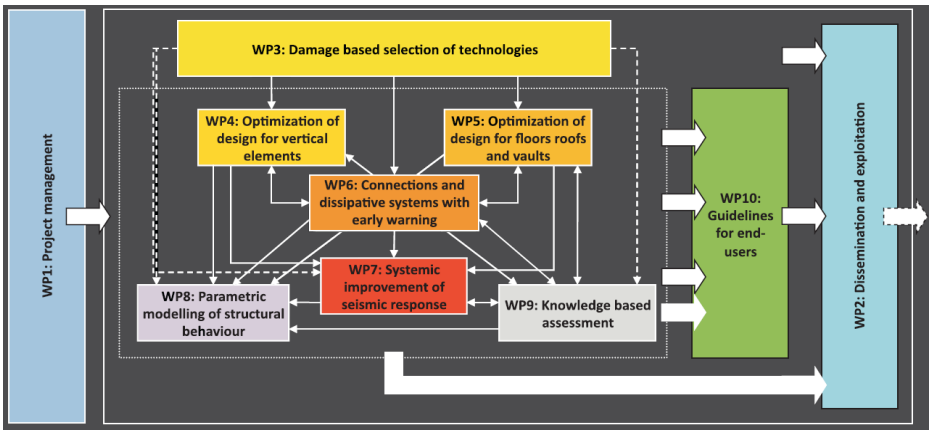

Figure 1. Schematic view of the project organization.

Earthquake-induced failure mechanisms, construction types and materials, intervention and assessment techniques have been cross-correlated with the aim of developing new integrated methodologies. Traditional materials have been complemented and enhanced by innovative industrial processes, and new high-performance elements have been developed. Advanced numerical studies carried out allowed to parameterize the results and to derive simple and optimized design procedures. Early warning techniques for smart interventions and advanced monitoring techniques have been also developed. From the several public deliverables produced, freely available at the project website [1], the five guidelines developed for end-users deserve special attention.

The NIKER results will allow increasing safety of buildings, reducing damage, and preserving cultural heritage value. Hence, on the long term, the proposed solutions improve sustainability and increase quality of life for the European citizens. Beside the more direct impact on the construction sector, other important impacts are expected to occur on economy, employment, tourism and all service-related activities.

The University of Minho (UMinho) played an important role inside the NIKER consortium, coordinating 2 of the work-packages and developing active research within the other work-packages. The contribution of UMinho to the most relevant project outcomes can be summarized as follows, see also Figure 2:

- Characterization of the in-plane cyclic behaviour of timber framed walls and definition of appropriate strengthening techniques for the timber joints (both experimental and numerical activities) [2];
- Development of an earth-based grout for injection of rammed earth walls (experimental activity) and characterization of structural rammed earth components under shear loading (both experimental and numerical activities) [3];
- Analysis of the bond durability of composite materials applied to masonry structures (both experimental and numerical activities) [4];
- Characterization of the cyclic behaviour of wall-to-floor connections (experimental activity) [5] and of wall-to-timber framed wall connections (both experimental and numerical activities) [6] [7].

(a)

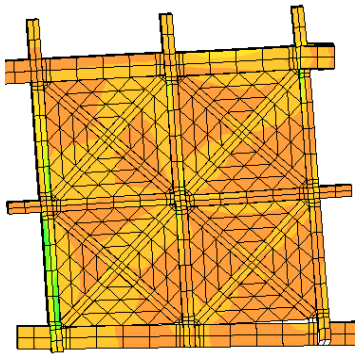

(b)

(c)

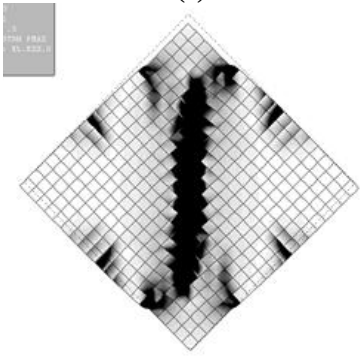

(d)

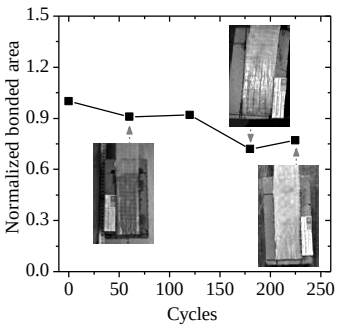

(e)

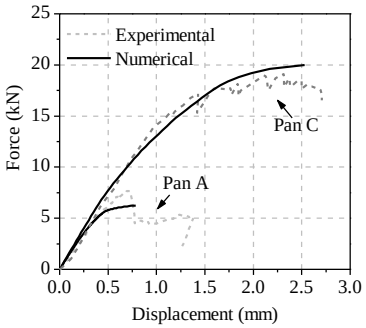

(f)

(g) (h) (i)

Figure 2. Main contribution from UMinho to the NIKER project: (a) and (b): timber framed walls; (c) and (d): rammed earth walls; (e) and (f): durability of composite materials; (g): wall-to-floor connections; (h) and (i): wall-to-timber framed wall connections.

Given the multitude of both experimental and numerical activities developed within the NIKER project at UMinho, this paper is therefore focused on two important structural components present in ancient masonry buildings and hardly studied in literature, namely timber framed walls and connections.

2 TIMBER FRAMED WALLS

This chapter describes the main results of an extensive experimental campaign carried out at UMinho dealing with the in-plane cyclic testing of full scale timber framed walls, aiming at characterizing their seismic performance and defining effective strengthening solutions. For further details, the reader is referred to [2].

2.1 Specimens and setup

The timber frames were built by specialized carpenters and masons. Real scale dimensions for the wall specimens were considered. Thus, the total length of the wall is 2.42 m and the total height 2.36 m, resulting in a height to length ratio of approximately 1, see Figure 3. The materials were adopted according to the Portuguese tradition, namely maritime pine (Pinus Pinaster) and bricks for masonry. In all of the connections a nail was inserted. Additionally, the materials components were tested according to the relevant standards and the main properties are listed in Table 1.

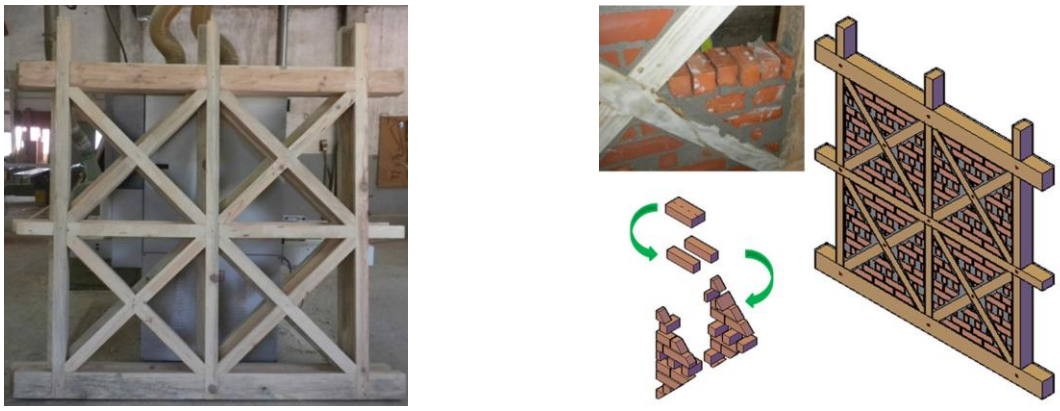

(a) (b)

Figure 3. Wall construction: (a) general view; (b) detail of the masonry infill.

Table 1. Average values of the material properties (CoV is given inside parentheses).

Material	wood	bricks	mortar	masonry
Compressive strength (MPa)	38.2 (12%) *// to grain*	34.5 (15%)	3.9 (13%)	7.5 (7%)
Flexural strength (MPa)	47.8 (28%)	---	1.6 (9%)	---
Shear strength (MPa)	---	---	---	0.2 (9%)

The cyclic tests were carried out using the setup illustrated in Figure 4. The application of the vertical load was done by means of vertical hydraulic actuators applied directly on the three posts of the walls in such a way that the actuators were able to follow the horizontal movement of the wall. The horizontal displacement was applied to the top timber beam through a hydraulic servo-actuator, so that cyclic displacements could be imposed to the top of the wall. Two different pre-compression load levels were considered, namely 25 kN/post and 50 kN/post. The displacement sequence applied was derived from a previous monotonic test performed on the wall in order to evaluate its displacement capacity. From the displacement of 10% of the maximum load and higher, each loading step was repeated three times. In total, ten unreinforced timber walls were tested, including timber walls without infill and walls filled with brick masonry. Further details are provided in [2].

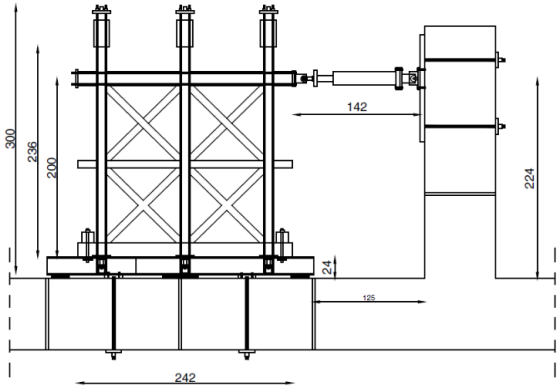

Figure 4. Scheme of the test apparatus.

2.2 Results

Figure 5 presents the horizontal force-displacement diagrams for two types of walls tested, namely brick masonry infill walls and timber frame walls, both submitted to the lower vertical load level. Complementary to the force-displacement curve, the evolution of the vertical displacements, measured by means of LVDTs placed in the posts at the base of the walls, is also shown.

In first place, it should be noted that all unreinforced timber frame walls with masonry infill subjected to a same vertical pre-compression level present a similar behaviour. Walls UIW25, tested with the lower vertical pre-compression load, present a predominant rocking behaviour, see Figure 5a, characterized by the well-known S-shape of the force–displacement diagrams [8], with a significant vertical uplift of the posts. The low vertical level applied in the wall, in conjunction with the aspect ratio of the walls (approximately 1), contributes to a great extent to the predominant flexural rocking mechanism. Also, the half-lap connection at the base of the wall revealed to be the vulnerable to tensile forces, given that only one nail was added. Notice that this trend for the uplift of the wall with the detachment of the post at the base is also observed in case of other typologies of cantilever shear walls, namely masonry walls, with the opening of horizontal cracks [8]. Once the connections were completely open, the walls exhibited a low decrease in terms of strength, since the bottom connections were not working anymore. This behaviour is typical of the rocking mechanism, for which high displacements can be reached with little reduction of strength.

If the shape of the hysteretic loops is compared with the uplift of the vertical posts for the same horizontal displacement, it can be noticed that: (1) the change in stiffness in the loading branch starts when the lateral posts start uplifting; (2) the plateau that occurred in the unloading branch of each cycle took place when the bottom connections start closing.

Timber frame walls with no infill exhibited a different behaviour in relation to the filled timber frame walls. The shear resisting mechanism predominated over the minor flexural component in the lateral response. But, as it can be noticed from the hysteretic diagram, the walls experienced severe pinching. This appears to indicate that pinching can partially be avoided by the infill. Moreover, the unloading branch of the various loops is more regular, even if the plateau characterizing the post uplifting is still present. The vertical uplift of the posts was minimal, if compared to that of the filled walls. For wall UTW25, see Figure 5b, once the wall failed (at an applied displacement of 30.4 mm), it was possible to observe an accommodation of the wall, which recuperated strength, even though stiffness degraded, managing to reach almost its maximum load. This resulted from a stress redistribution, after the failure

of the central connection, and stresses were redistributed to other connections, allowing the wall to regain strength.

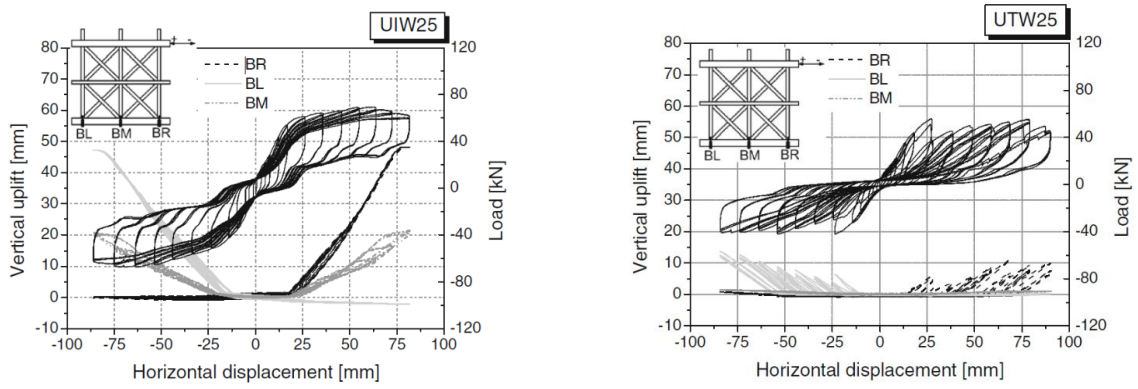

Figure 5. Hysteretic curves for two different timber frame walls: (a) brick masonry infill (lower vertical load level); (b) timber frame wall (lower vertical load level).

As it can be deduced from the analysis done until now, the presence of infill greatly changes the response of timber frame walls to cyclic actions.

3 EXPERIMENTS ON MASONRY TO TIMBER CONNECTIONS

The seismic vulnerability of unreinforced masonry (URM) buildings is well recognized in literature [9], as well as the importance of the connections between the main structural components. To act on the conservation of historical buildings, it is of major importance to study the behaviour of structural connections and to develop appropriate and engineered retrofitting solutions.

Two configuration of connections – wall-to-floor and wall-to-timber framed wall – were chosen as base of the experimental campaign and following analysis, carried out under the NIKER project and in collaboration with enterprise Monumenta. Construction details, materials and loading conditions of the specimens meant to replicate connections found in two typologies of URM buildings built during the 19th century, in Portugal (Pombalino Tardio and Gaioleiro), which are recognized for their seismic vulnerability. Further details on the experimental works can be found elsewhere [5] and [6].

3.1 Specimens and setup

The experimental campaign consisted of seventeen pull-out tests of wall-to-floor connections and seven tests of wall-to-timber framed wall connections. Both types of specimens included a rubble masonry wall as primary component. The walls are constituted by limestone of different sizes bonded with poor mortar joints. Full scale walls were 2.0 m long, 1.6 m high, and thickness was 0.4 m or 0.6 m. Further details on the setup can be found in [5] and [6].

Specimens representing wall-to-floor connections had a timber floor joist placed perpendicularly to the wall and nailed to a timber wall-plate built in along the wall (frechal). Each wall had two sets of timber floor joists and wall-plates, therefore two pull-out tests per wall were performed. The strengthening solution was developed in cooperation with Monumenta and consisted of a steel angle bolted to the floor joist, anchored to the wall by a tie rod with a squared anchor plate. On each end of the tie rod there was a stainless steel half-sphere in a cup, which was intended to work as a hinge.

For wall-to-timber framed wall connections, in the less conservative typology, the timber framed wall has no intermediate connections with the wall along its height, being the connection ensured by the floor joists at top and bottom. No timber elements were included in the specimens, and only the anchoring system was studied. The injection anchors were placed in pairs, in pre-drilled holes.

Considering laboratory limitations in terms of space as well as size of specimens, it was possible to develop a self-balanced test apparatus capable of redirecting the pull-out force back to the specimen, as shown in Figure 6. In order to simulate the compression state of the walls resulting from permanent loads, four hydraulic actuators were placed over rigid steel profiles on the top of the walls. Since the application of the strengthening and until testing, the compression state was kept constant (compression stresses of 0.2 MPa and 0.4 MPa, corresponding respectively to the walls' thickness of 0.4 m and 0.6 m).

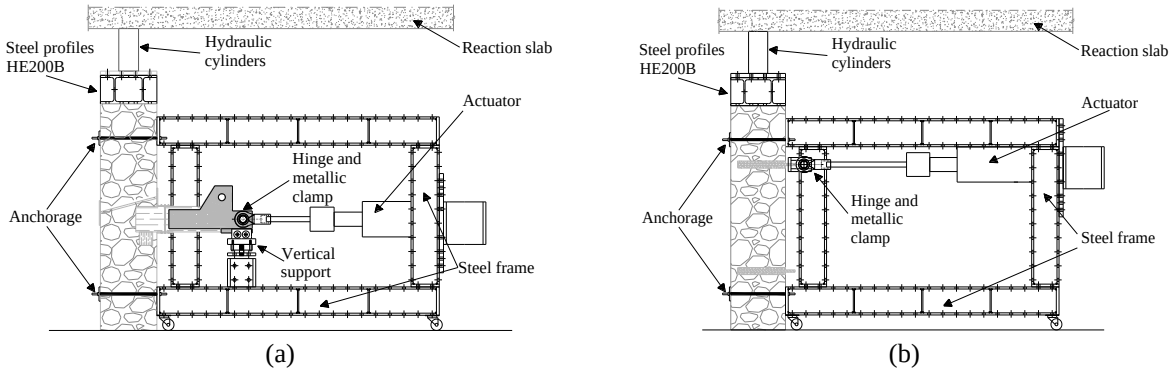

Figure 6. Test apparatus: (a) wall-to-floor pull-out; (b) wall-to-timber framed wall pull-out.

3.2 Results

3.2.1 Wall-to-floor connections

The main results of the eight quasi-static cyclic tests on strengthened wall to floor connections are listed in Table 2. The average values of the pull-out forces of the two thicknesses of walls are very close, being the one of the 0,4 m walls slightly higher, contrary to what was initially expected. This is possibly due to the fact that for the 0,6 m walls the masonry cone breakout did not occur. For the for 0,4 m walls, failure in all specimens resulted from the combination of masonry cone breakout with failure of the bolted connection, resulting in great similarity of the hysteresis loops [5]. The 0,6 m walls presented mainly failure of the bolted connection between the steel angle and the timber floor joist and yielding of the steel tie, but with similar hysteresis loops until failure. Specimens WF.60.A.3 and WF.60.A.4B had brittle failure modes, bending of the wood joist at the bolted connection, which broke completely, and failure of the steel rod. Specimens WF.60.A.2B and WF.60.A.3B failed by ripping of the wood joist at the bolted connection. Due to the variety in failure modes, the 0,6 m walls presented higher coefficients of variation than the ones obtained for the 0,4 m walls (bellow 10%).

Table 2. Main results for the experiments on strengthened wall-to-floor connections.

Specimen	F (kN)	Δ_y (mm)	Δ_u (mm)	μ
40.3A	93,09	0,98	91,47	93,7
40.3B	105,38	-	-	-
40.4A	94,50	0,80	84,32	105,9
40.4B	94,07	0,93	88,04	95,0
Average	96,8	0,9	87,9	98,2
CoV (%)	5	8	3	6
60.2B	92,42	2,97	21,74	7,3
60.3A	82,67	2,61	16,67	6,4
60.3B	100,65	4,59	45,52	9,9
60.4B	90,02	2,26	22,15	9,8
Average	91,4	3,1	26,5	8,4
CoV (%)	7	29	42	18

The yield displacement Δ_y, and the ultimate displacement Δ_u of the strengthening connections were estimated based on the joist/wall slip. The yield displacement was taken as the displacement when first yielding occurs, and the ultimate displacement corresponded to the displacement at the 100 mm step, for the 0,4 m walls, and to the post-peak displacement when a loss of 20% load carrying capacity happened [10], for the 0,6 m walls. In spite of this last criterion being more common, it was not possible to apply it to the 0,4 m walls because the required load carrying capacity loss was not obtained. The displacement ductility factor μ (ratio between Δ_u and Δ_y) determined for the 0,4 m walls is extremely high, because the connection is governed by slip, creating a plateau after yielding, see

Figure 7a. For the 0,6 m walls, the strengthened connection also displays ductility factors characteristic of ductile components, see also Figure 7b.

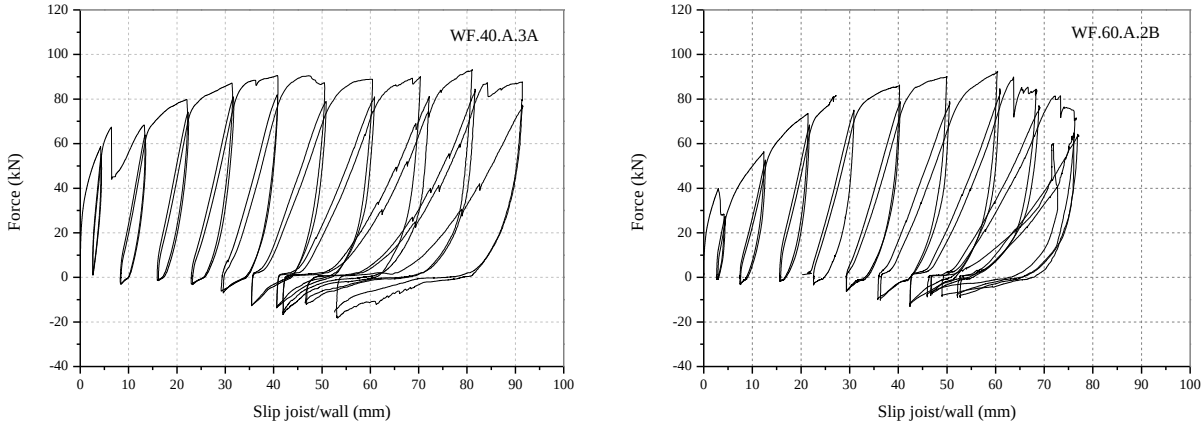

(a) (b)

Figure 7. Typical pull-out force-displacement curves for wall-to-floor connections: (a) 0.4 m thick wall; (b) 0.6 m thick wall

The similarity in force-displacement curves, particularly during the pre-peak phase, occurs because the connections were governed by the single shear bolted connection between the timber joist and the steel angle. These mechanisms are the crushing of the timber joist and shear failure of the bolts. The hysteretic behaviour encloses loss of strength between cycles, stiffness degradation and pinching, see Figure 7. Compression forces associated with load reversal are small, as result of the imposed test procedure. In all tests, there is a loss of force in the range of 20 kN to 70 kN because of the detachment of the steel angle from the timber joist. Tests from both 0,4 m and 0,6 m walls, dissipated most of their energy through the ripping of the wood joists, consequently there is not a big difference between them [5].

3.2.2 Wall-to-timber framed wall connections

The main results of the five quasi-static cyclic tests on strengthened wall-to-timber framed wall connections are presented in Table 3. There is a visible difference, approximately 30%, in the maximum pull-out force between tests conducted at the top and at the bottom of the wall. At the base of the wall the average maximum pull-out force was 107.9 kN, while at the top the same parameter reached 76.8 kN, both with a CoV below 5%.

The ultimate displacement was calculated in the same way as for the tests performed on wall-to-floor connections with a 0,6 m thick wall. Both yielding and ultimate displacements were obtained from the total slip (s_T), which is the relative displacement between the loaded end of the anchors and the back face of the wall. Specimens at the bottom of the wall have a smaller ductility factor than the ones at the top. The ductility factor determined for specimen WT.40.I.1D was very high when compared to the other specimens, probably due a different arrangement of the masonry and of the interface grout/masonry.

Table 3. Main results from the experiments on wall-to-timber framed wall strengthened connections.

Specimen	F (kN)	Δ_y (mm)	Δ_u (mm)	μ
WT.40.I.1A	111,7	2,5	6,8	2,7
WT.40.I.2A	107,2	-	-	-
WT.40.I.2B	104,9	2,7	9,5	3,5
Bottom average	107,9	2,6	8,2	3,1
CoV (%)	3	5	24	18
WT.40.I.1D	81,2	0,7	12,1	18,6
WT.40.I.2C	75,0	0,9	6,7	7,4
Top average	76,8	1,5	10,8	9,4
CoV (%)	4	75	43	67

Force-displacement hysteresis loops of specimens WT.40.I.1A and WT40.I.2C represent the typical curves of tests performed at the bottom and top of the wall, respectively, see also Figure 8. The pinched hysteresis loops show a great similarity, being controlled by bond slip phenomena at the grout/masonry interface. The cyclic behaviour shows a strength and stiffness degradation with the increasing steps and an accumulation of residual displacements. The descending branches of the cycles pushed the specimen as much as 0.5 mm, which caused the development of compressive forces. The values of this force obtained for top and bottom of the walls were very close (21.0 kN and 23.9 kN), not portraying the clear distinction noticed for tension. Residual displacements and compression forces depend greatly on the composition of the interface grout/masonry and surrounding masonry.

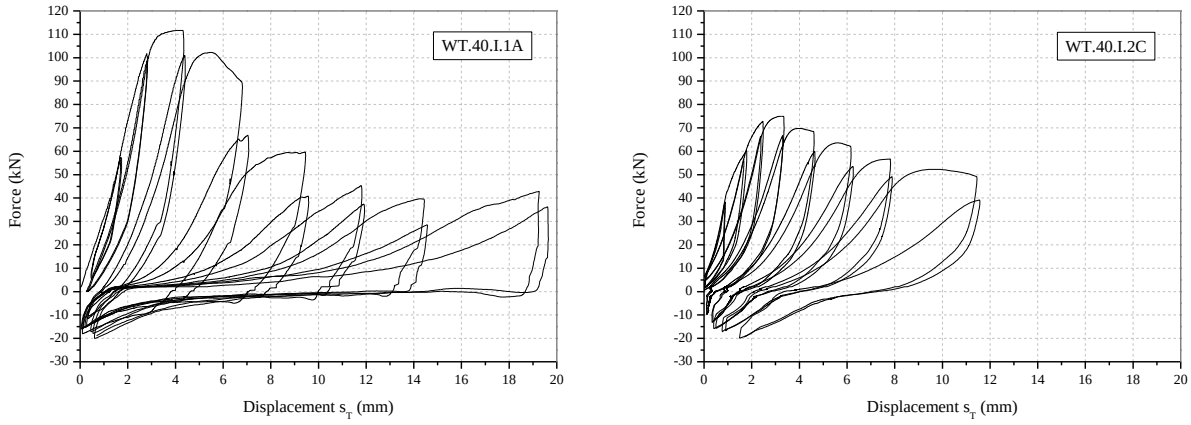

(a) (b)

Figure 8. Typical pull-out force-displacement curves for injection anchors: (a) bottom part; (b) top part.

All tests showed combined cone-bond failure with sliding at the interface grout/masonry and masonry breakout. Tests at the top showed a higher influence of the masonry cone while tests at the bottom showed bond failure at the grout/masonry interface as the major contributor for failure.

Differences between tests performed at the top and bottom of the wall are most probably due to different boundary conditions. Lower out-of-plane displacements of the walls, higher pull-out force, lower ductility and shape of the force-displacement curves support the explanation that the bottom of the wall behaves like a fixed support, while the top resembles a pinned support.

4 MODELLING OF STRENGTHENED WALL-TO-TIMBER FRAMED WALL CONNECTIONS

This chapter discusses the most relevant results derived from the numerical modelling of the experimental tests on wall-to-timber framed wall connections, presented in section 3.2.2, in particular the upper level anchorages. Further details on the modelling work are given elsewhere [7].

4.1 Numerical model

A detailed 3D finite element model was developed in DIANA 9.4 [11] aiming at an accurate description of the structural behaviour of the injected anchors. Three-dimensional volume elements were used for the mesh since an precise stress distribution is relevant for a clear understanding of the stress field and of the structural behaviour, see Figure 9a. In order to simulate the behaviour of the different failure mechanisms, the model includes also interface elements around the steel bar (inner interface) and between the grout and the masonry (outer interface). Figure 9b illustrates the modelling strategy used for the numerical simulation of the anchoring system. The model is fully restrained at the bottom in order to reproduce the experimental setup. The areas of the wall in contact with the reaction frame were restrained only for horizontal out-of-plane displacements.

Masonry was assumed as a homogeneous isotropic material with mean-value properties, which is a good compromise between accuracy and efficiency. Table 4 provides the elastic properties adopted for the materials. The interface stiffness was defined according to the available literature. Here, studies in the field of concrete-steel bond behaviour in reinforced concrete were taken as an approximation. A

range of values around 9-400 MPa/mm, depending on the bond conditions, has been indicated for the tangential stiffness of the inner interface according to investigations in this field.

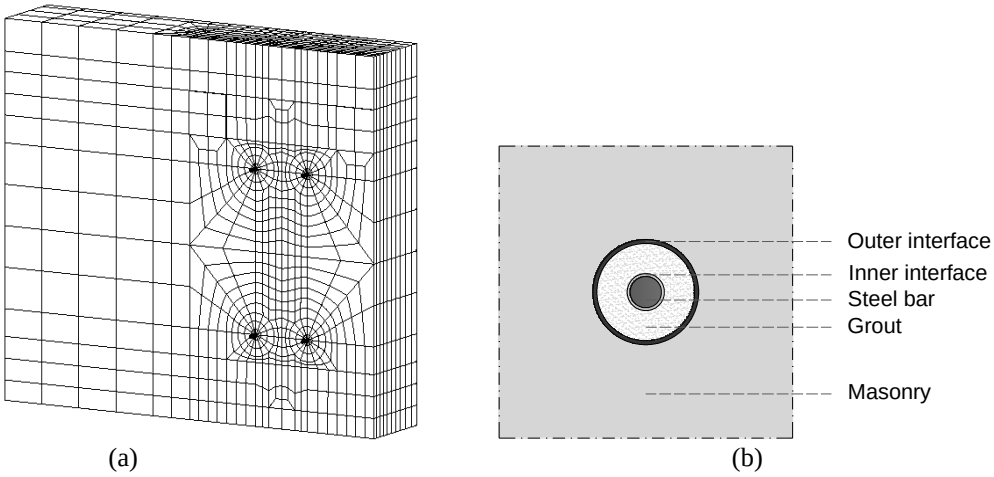

Figure 9. Numerical model: (a) 3D mesh; (b) detail of the anchor modelling.

A number of investigations on the behaviour of grout-masonry interfaces were performed considering different masonry types. Bajer and Barnat [12] carried out experimental tests and numerical analyses for the study of the glue-concrete interface of bonded anchors under tensile load and a value around 500 MPa/mm was pointed out for the shear stiffness. The bond between grout and surrounding brick masonry was investigated by Gigla [13], providing values between 55 MPa/mm and 66 MPa/mm for the shear stiffness. Literature studies concerning unit-mortar interface on masonry (which can be also associated to the grout-masonry bond), as well as some expressions for its calculation, were also considered to estimate the interface parameters. Thus, a range of values around 10-500 MPa/mm seems reasonable for the outer tangential stiffness. The usual elasticity equations relating normal and tangential stiffness indicate that the normal stiffness is approximately twice the tangential one.

Table 4. Properties of the materials used.

	E (GPa)	ν (-)	γ (kg/m^3)
Masonry	1.0	0.2	1900
Steel bar	210.0	0.3	7850
Grout	30.0	0.2	2300
HE200 B profile	210.0	0.3	7850

4.2 Analysis and validation

The experimental test procedure was followed for the numerical analysis, where the compressive vertical load was applied on the top of the metallic beam and an upper pair of anchors was loaded in tension by applying increasing horizontal displacements at its end. A set of linear elastic analysis was carried out first in order to calibrate suitable interface stiffness values that best match the experimental curves in the linear range. This inverse fitting process resulted in the values presented in Table 5, which are within the range defined in literature.

The non-linear behaviour of the masonry is modelled by adopting two constitutive models based on the total strain crack model: the total strain fixed crack model (FCM) and the total strain rotating crack model (RCM). In both models a crack is initiated when the maximum principal stress equals the tensile strength of the material and the initial orientation of the crack is normal to the maximum principal strain. In the fixed crack model the strain transformation matrix is fixed upon cracking and the crack plane is also fixed during the full analysis process. On the other hand, in the rotating crack model the crack direction rotates with the principal strain axes ensuring that the crack remains normal

to the direction of the maximum principal strain. The rotating crack model is more flexible and allows a gradual correction of an initially mispredicted crack direction.

Table 5. Interface stiffness values calibrated.

Inner Interface		Outer Interface	
Tangential stiffness	Normal stiffness	Tangential stiffness	Normal stiffness
100	200	50	100

In the fixed crack model, a shear retention factor has to be chosen for the definition of the shear behaviour, which leads to some stress built-up and locking. On the contrary, in the rotating crack model the shear stiffness is evaluated during the analysis and updated taking into account the current damage state [14]. It is expected that the structural behaviour of the model becomes highly dependent on the shear behaviour of masonry. Therefore, both formulations were adopted and analysed, aiming at discussing the most suitable approach for this type of problems.

Most of the non-linearities are expected to concentrate in the masonry, since at the time masonry fails, steel and grout are most probably still in the linear range. Therefore, the non-linear behaviour of the grout was not considered in this work because almost no damage was observed during the experimental tests. As such, only masonry is considered with non-linear behaviour in the present model. Masonry is modelled using exponential softening in tension and a parabolic strain-stress relationship in compression, for both fixed and rotating formulations. While shear behaviour does not require the user definition within the rotating crack model, in the fixed crack model the post-cracked shear behaviour was modelled using a constant shear retention factor. The nonlinear properties for the masonry constitutive models definition were estimated based on recommendations from literature [15]. The adopted values for the definition of the nonlinear constitutive models for masonry are summarized in Table 6.

Table 6. Non-linear parameters adopted for the masonry.

Compression		Tensile		Shear
f_c (MPa)	G_c (N/mm)	f_t (MPa)	G_t (N/mm)	β*
1.74	2.80	0.10	0.05	0.01

*Shear factor only for the fixed crack model

The force-displacement curves coming from the FCM and RCM are depicted in Figure 10, as well as the experimental envelope obtained from the force-displacement curves of three tests. The comparison of the numerical analyses (FCM and RCM) against the experimental envelope does not show significant differences concerning the linear behaviour and peak force, as expected. Although both numerical curves present a sudden decrease in load capacity just after the peak, the post-peak response exhibits considerable differences. The FCM formulation provides a continuously increase of the force after peak, which is not in agreement with experiments. In fact, the experimental post-peak envelope shows clearly a gradual force decrease with respect to displacement, which is well captured by the RCM formulation. This last approach provides a maximum force of 69 kN (90% of the average experimental value) and an ultimate displacement of 15 mm.

Figure 10 shows clearly that the shear modelling can have a great influence on the post-peak behaviour of this type of structures, making the difference between a realistic structural modelling of the system and an incorrect overestimation of strength, even if the first peak is independent of the model.

To further discuss the structural behaviour, the tensile principal strains are plotted and analysed as an indicator of damage. Figure 11 shows the maximum principal strains at peak load, for both constitutive laws. The distribution of damage is very similar for both models in the surrounding areas of the anchors, although it is more severe in the FCM. The top cross section shows damage along the anchors for the FCM while diagonal strain concentrations were found for the RCM. In both analyses the crack pattern is characterized by the formation of a shear cone on masonry and sliding trough the

external interface, more noticeable in FCM. Experimental tests showed an influence of the masonry cone much higher than the interface grout/masonry, as the main contributor for failure. Thus, the RCM model seems to better describe the behaviour verified during the experimental tests. The analysis of damage concentration in the post-peak behaviour (not presented here, as the differences are small) confirms the shear cone in the masonry for both FCM and RCM formulations, although more evident in the last case. The strain distribution and obtained failure modes of these analyses further validate the RCM model.

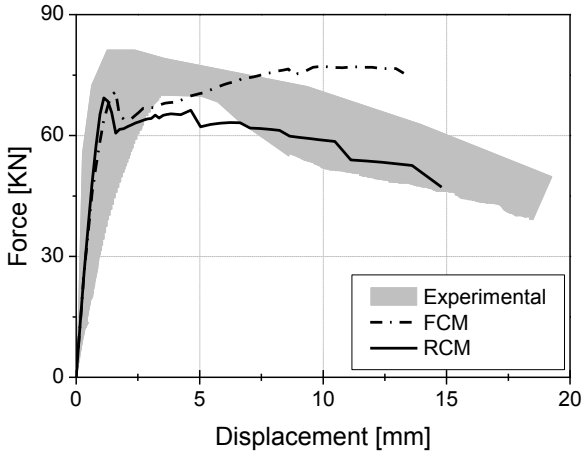

Figure 10. Force-displacement curves for the RCM and FCM formulations and experimental envelope.

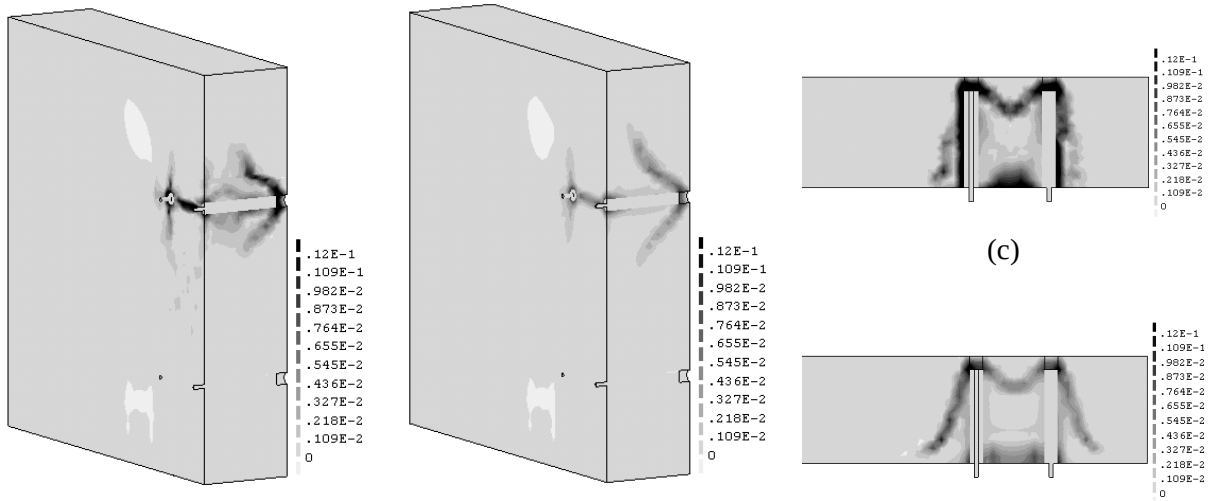

Figure 11. Maximum principal strains depicted at vertical and horizontal cross sections for peak load: (a) FCM; (b) RCM; (c) FCM; (d) RCM

5 FINAL REMARKS

This paper introduces the most relevant experimental and numerical activities carried out at UMinho within the NIKER and discusses some of the results associated to two innovative research topics inside the project: performance of timber framed walls and behaviour of masonry to timber connections.

As for the timber framed walls, the presence of infill changes considerably the response of the walls in terms of predominant resisting mechanism, ranging from a predominant flexural or mixed shear/flexural behaviour of infill timber frame walls to a shear predominant resisting mode for timber frame walls with no infill. Also, bare timber frame walls present lower load capacity, stiffness and ductility when compared to infill walls.

With regard to the experiments on masonry to timber connections, the failure modes obtained for the strengthened wall-to-floor connections were within the behaviour predicted prior to the experimental campaign. Combination of masonry cone breakout with failure of the bolted connection was observed for all tests on the 0.4 m walls, while failure of the bolted connection and yielding of the steel rod occurred in tests on the 0.6 m walls. The high ductility of the strengthening is associated with the combined behaviour of the wood joist, the bolted connection and the steel angle, which display high deformations.

As for the wall-to-timber framed wall connections, boundary conditions seem to have provided a distinct behaviour between anchors at the top and bottom of the wall in terms of force-displacement curve, maximum pull-out force, and failure mode type. Tests at the top showed a 30% decrease of the pull-out force. All tests showed combined cone-bond failure, with higher contribution of the bond slip in the tests performed at the bottom and higher participation in failure of the cone breakout in tests performed at the top. The compressive stress of the wall influenced the behaviour of the injection anchors, which was especially noted with the contribution of internal friction in the softening branch of the curve.

In terms of the modelling of the structural behaviour of masonry wall-to-timber framed walls, the model was calibrated and validated against the available experimental results. The rotating crack model (RCM) showed a better agreement regarding the post-peak behaviour, since the shear strength is updated after cracking along the complete analysis. Also the RCM damage pattern observed during the analysis was more compatible with the failure mode observed experimentally.

ACKNOWLEDGMENTS

The work presented in this paper was been funded by project FP7-ENV-2009-1-244123-NIKER of the 7th Framework Programme of the European Commission, which is gratefully acknowledged. Authors would like to thank the technical staff of Civil Engineering laboratory from Universidade do Minho for the assistance provided. Thanks are also due to Monumenta, also partner of the NIKER project, for the valuable collaboration in several experimental activities, and to Cintec® for the installation of the injection anchors.

REFERENCES

[1] Website of the Niker project, www.niker.eu

[2] Poletti, E. (2013) Characterization of the seismic behaviour of traditional timber frame walls, PhD Thesis, University of Minho, available at http://hdl.handle.net/1822/28845

[3] Silva, R. (2013) Repair of earth constructions by means of grout injection, PhD Thesis, University of Minho, available at http://hdl.handle.net/1822/28793

[4] Ghiassi, B. (2013) Durability analysis of bond between composite materials and masonry substrates, PhD Thesis, University of Minho, available at http://hdl.handle.net/1822/28878

[5] Moreira, S., Ramos, L.F., Oliveira, D.V., Lourenço, P.B., Mateus, L. (2014) Developing a seismic retrofitting solution for wall-to-floor connections of URM buildings with wood diaphragms, 9th International Masonry Conference, Guimarães, Portugal, CD-ROM.

[6] Moreira, S.M., Ramos, L.F., Oliveira, D.V., Lourenço, P.B. (2014) Experimental behavior of masonry wall-to-timber elements connections strengthened with injection anchors, Engineering Structures, accepted for publication.

[7] Araújo, A.S., Oliveira, D.V., Lourenço, P.B. (2014) Numerical study on the performance of improved wall-to-wall connections in traditional masonry buildings, Engineering Structures, accepted for publication.

[8] Magenes, G., Calvi, G.M. (1997) In-plane seismic response of brick masonry walls. Earthq Eng Struct Dyn, 26, 1091-1112.

[9] Bruneau, M. (1994) State-of-the-art report on seismic performance of unreinforced masonry buildings. Journal of Structural Engineering, 120(1), 230-251.

[10] Park, R. (1989) Evaluation of ductility of structures and structural assemblages from laboratory testing. Bull New Zeal Soc Earthq Eng., 22(2), 155–166.

[11] DIANA 9.4 (2009), DIANA, DIsplacement method ANAlyser, release 9.4, User's Manual.

[12] Bajer, M., Barnat, J. (2012) The glue–concrete interface of bonded anchors. Construction and Building Materials, 34, 267–274.

[13] Gigla, B. (2004) Bond strength of injection anchors as supplementary reinforcement inside historic masonry. 13th International Brick and Block Conference, 119–128.

[14] Rots, J. G. (1988) Computational modeling of concrete fracture, PhD Thesis.

[15] Lourenço, P.B. (2009) Recent advances in masonry modelling: micromodelling and homogenisation. Multiscale modeling in solid mechanics computational approaches, Imperial College Press, 251–294.